Supplementary Materials

Characterization methodology

X-ray powder diffraction (XRD) was carried out on a D8 Advance X-ray powder diffractometer. Fourier transform infrared (FTIR) spectroscopy analysis was carried out on a FTIR-650 spectrometer. Ultraviolet-visible (UV-vis) diffuse reflectance spectroscopy (DRS) measurement was done on a TU-1901 double beam spectrophotometer. X-ray photoelectron spectroscopy (XPS) investigation was performed an AXIS Supra X-ray photoelectron spectrometer. Scanning electron microscopy (SEM) observation was performed on a JSM-6701F field-emission scanning electron microscope. Transmission electron microscopy (TEM) analysis was performed on a JEM-F200 field-emission transmission electron microscope. Electron paramagnetic resonance (EPR) signals were monitored on a Bruker microESR spectrometer. Liquid chromatography-mass spectrometry (LC-MS) analysis was performed on a thermos TSQ Quantum Ultra mass spectrometer and Agilent 1100 liquid chromatograph.

Photoelectrochemical measurement

The photocurrent response spectra and electrochemical impedance spectroscopy (EIS) spectra of the samples were obtained using a CST 350 electrochemical workstation. A three-electrode cell configuration was used for the photoelectrochemical testing, where a platinum foil electrode and a standard calomel electrode (SCE) were used as the counter electrode and reference electrode, respectively. To prepare the working electrode, 15 mg of the photocatalyst, 0.75 mg of acetylene black and 0.75 mg of poly-vinylidene fluoride (PVDF) were uniformly mixed using 1-methyl-2-pyrrolidione (NMP) as the solvent. The formed slurry mixture was uniformly coated onto a fluorine-doped tin oxide (FTO) glass substrate with an effective area 1×1 cm^2, followed by 5 h of drying at 60 ^{o}C. 0.1 M Na_2SO_4 aqueous solution was used as the electrolyte. A PLS-SXE300BF 300 W xenon lamp was employed as the light source to generate simulated sunlight. The photocurrent response was measured at a bias potential of 0.2 V. EIS measurements were conducted by applying a sinusoidal voltage pulse with amplitude of 5 mV over a frequency range of 10^{-2} to 10^{5} Hz.

DFT calculation

The calculations of geometry configurations and the band structures were carried out by the Vienna ab-inito simulation package (VASP), taking advantage of the density-functional theory (DFT) in Perdew-Burke-Ernzerhof (PBE) generalized gradient approximation (GGA). SCF convergence criteria was set to be 10^{-5} eV and the relaxation convergence criteria was set to be 0.03 eV $Å^{-1}$ in the calculation. An energy cutoff of 400 eV was used for the plane-wave expansion of the electronic wave function. BOB (012) crystal plane was built from the optimized BOB unit cell with lattice parameters of a = b = 3.93219 Å, c = 8.51622 Å, α = β = γ = 90.0000° and the corresponding 9 × 3 × 1 k-point mesh was modeled in the calculations. AMO (220) crystal plane was built from the optimized AMO nanosheet unit cell with lattice parameters of a = b = c = 9.2588 Å, α = β = γ = 90.0000° and the corresponding 5 × 5 × 1 k-point mesh was modeled in the calculations.

Table S1. Comparison of the photocatalytic performance of 20%AMO/BOB with that of previously reported AMO- or BOB-based composite photocatalysts towards the degradation of MB.

Samples	Light sources	$C_{photocatalyst}$	MB	Irradiation time (min)	η	References
20%Ag_2MoO_4/BiOBr	300-W Xe lamp	0.5 g L^{-1}	10 mg L^{-1}	30	93.8%	This work
5%Ag_2MoO_4/Ag_3PO_4	350-W xenon lamp with a 420 nm ultraviolet filter	0.5 g L^{-1}	10 mg L^{-1}	15	94%	[1]
Ag_2MoO_4/AgBr	410 nm LED irradiation	1 g L^{-1}	20 mg L^{-1}	6	88%	[2]
Bi_2MoO_6/Ag_2MoO_4	tungsten lamp of 25W/m^2	-	10 mg L^{-1}	140	91.8%	[3]
60%α-Ag_2MoO_4/WO_3	300-W Xe lamp (λ > 420 nm)	0.5 g L^{-1}	0.5 g L^{-1}	150	68%	[4]
30wt%Ag_2MoO_4/$Bi_4Ti_3O_{12}$	simulated sunlight emitted from a 300-W xenon lamp	1 g L^{-1}	5 mg L^{-1}	15	98.3%	[5]
40%g-C_3N_4/Ag_2MoO_4	410 nm LED light (50 W)	1 g L^{-1}	20 mg L^{-1}	12	99.5%	[6]
Ag/AgCl/Ag_2MoO_4	300-W Xe lamp with a cut-off filter (λ > 420 nm)	0.6	MB (10 mg L^{-1})	90	98.3	[7]
BiOBr-M	300-W Xe lamp	0.5 g L^{-1}	4 × 10^{-5} mol L^{-1}	36	92%	[8]
BiOBr lamellas	350-W Xe lamp with a 420 nm ultraviolet filter	0.4 g L^{-1}	5 mg L^{-1}	450	50%	[9]
40%BiOCl/BiOBr	visible LED light irradiation	0.6 g L^{-1}	10 mg L^{-1}	360	93%	[10]
$Bi_4O_5Br_2$/BiOBr	blue light (405 nm, 20 W)	1.58 g L^{-1}	80 mg L^{-1}	100	36%	[11]
BiOBr/Ag_2CrO_4 (2:1)	500 W xenon	0.5 g L^{-1}	10 mg L^{-1}	20	98.3%	[12]

	lamp equipped with a 420 nm filter					
3%p-C_3N_4/f-BiOBr	250-W Xe lamp with a 400 nm cut-off filter	1 g L^{-1}	25 mg L^{-1}	100	94.3%	[13]
Ag_3PO_4/RGO/BiOBr	high pressure mercury lamp with a 420nm cutoff filter	0.5 g L^{-1}	20 mg L^{-1}	60	96.5%	[14]
20%$CuBi_2O_4$/Bi/BiOBr	500 W Xenon lamp with a UV-cutoff filter ($\lambda > 420$ nm)	1 g L^{-1}	20 mg L^{-1}	120	73%	[15]
BiOBr/$Ag_6Si_2O_7$ (5:1)	300 xenon lamp and a 400 nm cutoff filter	1 g L^{-1}	20 ppm	15	98%	[16]

References

1. Cao, W.; An, Y.; Chen, L.; Qi, Z. Visible-light-driven Ag_2MoO_4/Ag_3PO_4 composites with enhanced photocatalytic activity. *J. Alloy. Compd.* **2017**, *701*, 350–357.

2. Wang, Z.; Zhang, J.; Lv, J.; Dai, K.; Liang, C. Plasmonic Ag_2MoO_4/AgBr/Ag composite: excellent photocatalytic performance and possible photocatalytic mechanism. *Appl. Surf. Sci.* **2017**, *396*, 791–798.

3. Balasurya, S.; Das, A.; Alyousef, A.A.; Alqasim, A.; Almutairi, N.; Khan, S.S. Facile synthesis of Bi_2MoO_6-Ag_2MoO_4 nanocomposite for the enhanced visible light photocatalytic removal of methylene blue and its antimicrobial application. *J. Mol. Liq.* **2021**, *337*, 116350.

4. Guo, R.; Han, G.; Yan, A.; He, Y.; Su, N.; Liu, X.; Yi, T. Epitaxial growth of metastable phase α-Ag_2MoO_4 on WO_3 surface: Visible light-driven photocatalysis, sterilization, and reaction mechanism. *J. Alloy. Compd.* **2020**, *814*, 152255.

5. Cheng, T.T.; Gao, H.J.; Sun, X.F.; Xian, T.; Wang, S.F.; Yi, Z.; Liu, G.R.; Wang, X.X.; Yang,

H. An excellent Z-scheme $Ag_2MoO_4/Bi_4Ti_3O_{12}$ heterojunction photocatalyst: construction strategy and application in environmental purification. *Adv. Powder Technol.* **2021**, *32*, 951–962.

6. Huo, Y.; Wang, Z.; Zhang, J.; Liang, C.; Dai, K. Ag SPR-promoted 2D porous g-C_3N_4/Ag_2MoO_4 composites for enhanced photocatalytic performance towards methylene blue degradation. *Appl. Surf. Sci.* **2018**, *459*, 271–280.

7. Jiao, Z.; Zhang, J.; Liu, Z.; Ma, Z. $Ag/AgCl/Ag_2MoO_4$ composites for visible-light-driven photocatalysis. *J. Photochem. Photobio. A* **2019**, *371*, 67–75.

8. Wang, X.; Zhang, Y.; Xu, H.; Ji, X.; Gan, L.; Zhang, R. Sugar-regulated bismuth oxybromide flowers with active imprinting sites for efficient photooxidative ability. *J. Alloy. Compd.* **2021**, *879*, 160374.

9. Li, H.; Liu, J.; Liang, X.; Hou, W.; Tao, X. Enhanced visible light photocatalytic activity of bismuth oxybromide lamellas with decreasing lamella thicknesses. *J. Mater. Chem. A* **2014**, *2*, 8926.

10. Zhang, J.; Lv, J.; Dai, K.; Liang, C.; Liu, Q. One-step growth of nanosheet-assembled BiOCl/BiOBr microspheres for highly efficient visible photocatalytic performance. *Appl. Surf. Sci.* **2018**, *430*, 639–646.

11. Budnyak, T.M.; Onwumere, J.; Pylypchuk, I.V.; Jaworski, A.; Chen, J.; Rokicinska, A.; Lindstrom, M.E.; Kustrowskic, P.; Sevastyanova, O.; Slabon, A. LignoPhot: Conversion of hydrolysis lignin into the photoactive hybrid lignin/$Bi_4O_5Br_2$/BiOBr composite for simultaneous dyes oxidation and Co^{2+} and Ni^{2+} recycling. *Chemosphere* **2021**, *279*, 130538.

12. Liu, X.; Wang, Y.; Kang, Y. In situ synthesis of novel high-efficiency visible-light-driven p-n heterojunction BiOBr/Ag_2CrO_4 photocatalysts. *Mater. Lett.* **2022**, *313*, 131714.

13. Ma, Z.; Deng, L.; Fan, G.; He, Y. Hydrothermal synthesis of p-C_3N_4/f-BiOBr composites with highly efficient degradation of methylene blue and tetracycline. *Spectrochim. Acta A* **2019**, *214*, 103–110.

14. Zhang, R.; Han, Q.; Li, Y.; Cai, Y.; Zhang, T.; Liu, Y.; Zhu, X. Fabrication of a Ag_3PO_4/Reduced graphene oxide/BiOBr ternary photocatalyst for enhanced visible-light photocatalytic activity and stability. *J. Alloy. Compd.* **2019**, *810*, 151868.

15. Fu, S.; Zhu, H.; Huang, Q.; Liu, X.; Zhang, X.; Zhou, J. Construction of hierarchical $CuBi_2O_4$/Bi/BiOBr ternary heterojunction with Z-scheme mechanism for enhanced broad-spectrum photocatalytic activity. *J. Alloy. Compd.* **2021**, *878*, 160372.

[16] Jia, K.L.; Zhu, Z.S.; Qu, J.; Jing, Y.Q.; Yu, X.J.; Abdelkrim, Y.; Hao, S.M.; Yu, Z.Z. BiOBr/$Ag_6Si_2O_7$ heterojunctions for enhancing visible light catalytic degradation performances with a sequential selectivity enabled by dual synergistic effects. *J. Colloid Interf. Sci.* **2020**, *561*, 396–407.

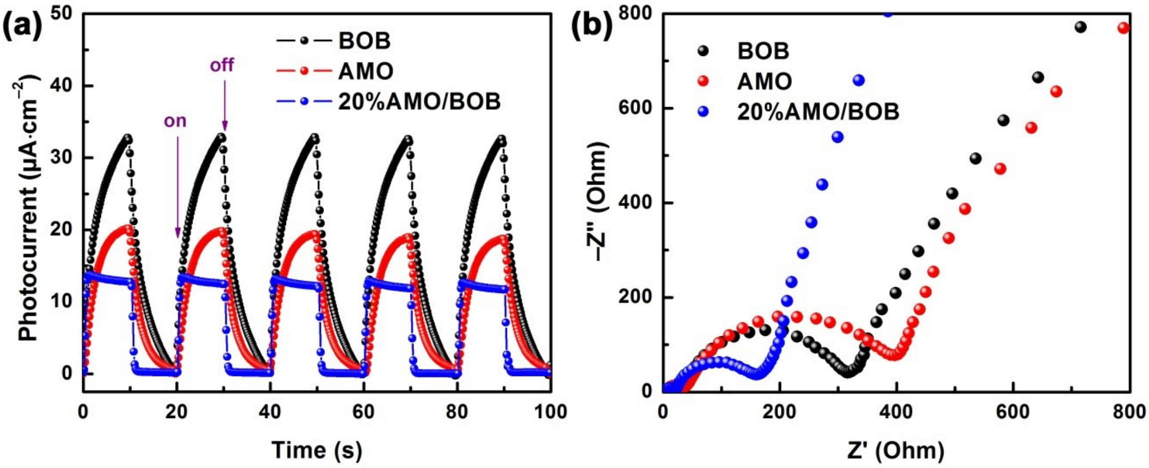

Fig. S1. Photocurrent response spectra (a) and EIS spectra (b) of AMO, BOB and 20%AMO/BOB.

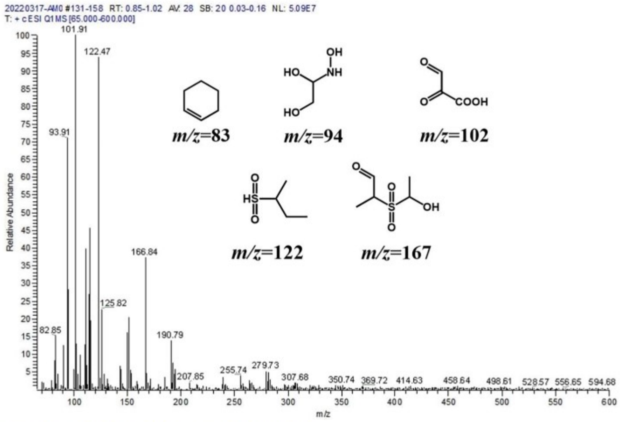
20220317-AM0 #131-158 RT: 0.85-1.02 AV: 28 SB: 20 0.03-0.16 NL: 5.09E7
T: + c ESI Q1MS [65.000-600.000]
m/z=83
m/z=94
m/z=102
m/z=122
m/z=167
Relative Abundance
m/z

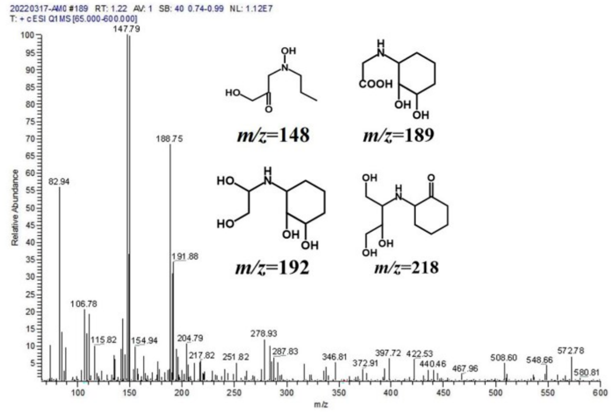
20220317-AM0 #189 RT: 1.22 AV: 1 SB: 40 0.74-0.99 NL: 1.12E7
T: + c ESI Q1MS [65.000-600.000]
m/z=148
m/z=189
m/z=192
m/z=218
Relative Abundance
m/z

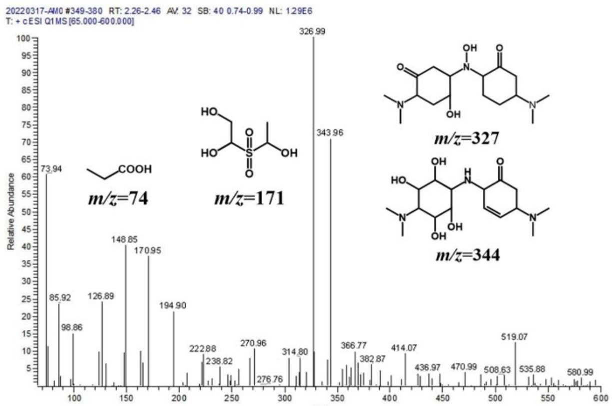
20220317-AM0 #349-380 RT: 2.26-2.46 AV: 32 SB: 40 0.74-0.99 NL: 1.29E6
T: + c ESI Q1MS [65.000-600.000]
m/z=74
m/z=171
m/z=327
m/z=344
Relative Abundance
m/z

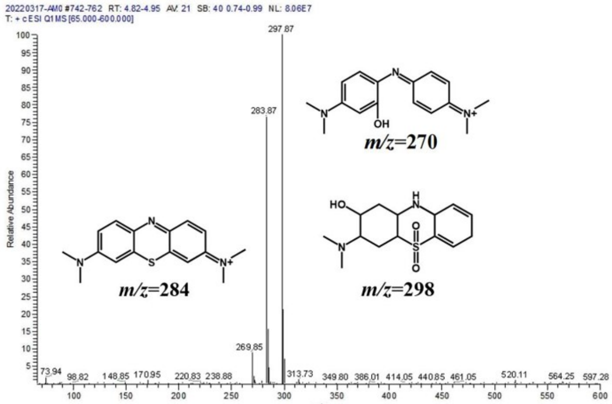
20220317-AM0 #742-762 RT: 4.82-4.95 AV: 21 SB: 40 0.74-0.99 NL: 8.06E7
T: + c ESI Q1MS [65.000-600.000]
m/z=270
m/z=284
m/z=298
Relative Abundance
m/z

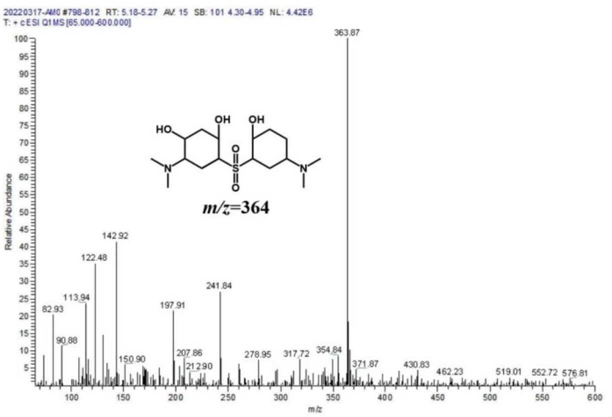
20220317-AM0 #798-812 RT: 5.18-5.27 AV: 15 SB: 101 4.30-4.95 NL: 4.42E6
T: + c ESI Q1MS [65.000-600.000]
m/z=364
Relative Abundance
m/z

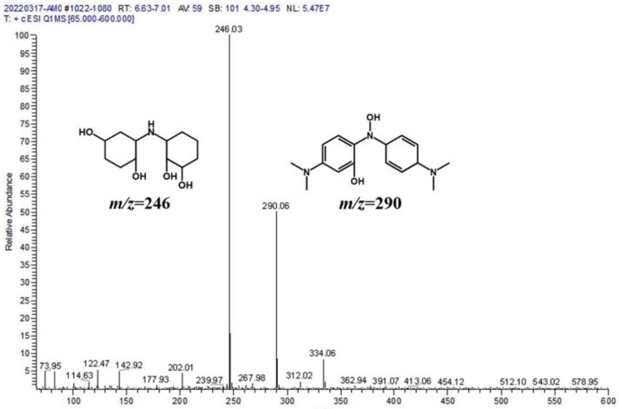
20220317-AM0 #1022-1080 RT: 6.63-7.01 AV: 59 SB: 101 4.30-4.95 NL: 5.47E7
T: + c ESI Q1MS [65.000-600.000]
m/z=246
m/z=290
Relative Abundance
m/z

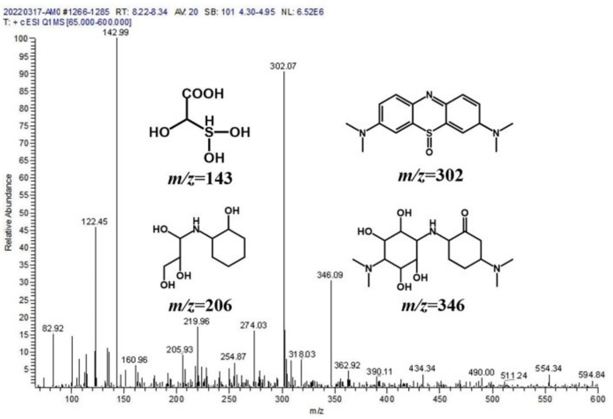
20220317-AM0 #1266-1285 RT: 8.22-8.34 AV: 20 SB: 101 4.30-4.95 NL: 6.52E6
T: + c ESI Q1MS [65.000-600.000]
m/z=143
m/z=302
m/z=206
m/z=346
Relative Abundance
m/z

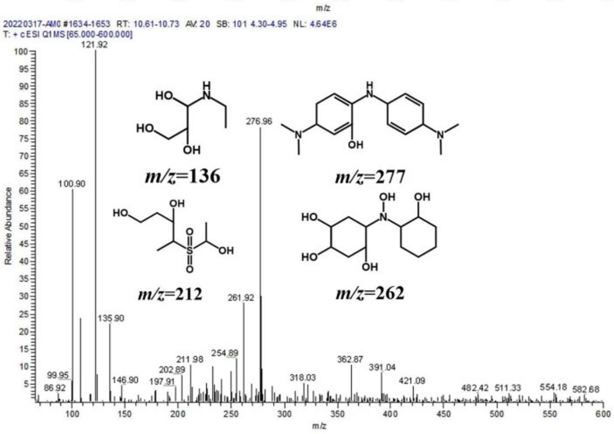
20220317-AM0 #1634-1653 RT: 10.61-10.73 AV: 20 SB: 101 4.30-4.95 NL: 4.64E6
T: + c ESI Q1MS [65.000-600.000]
m/z=136
m/z=277
m/z=212
m/z=262
Relative Abundance
m/z

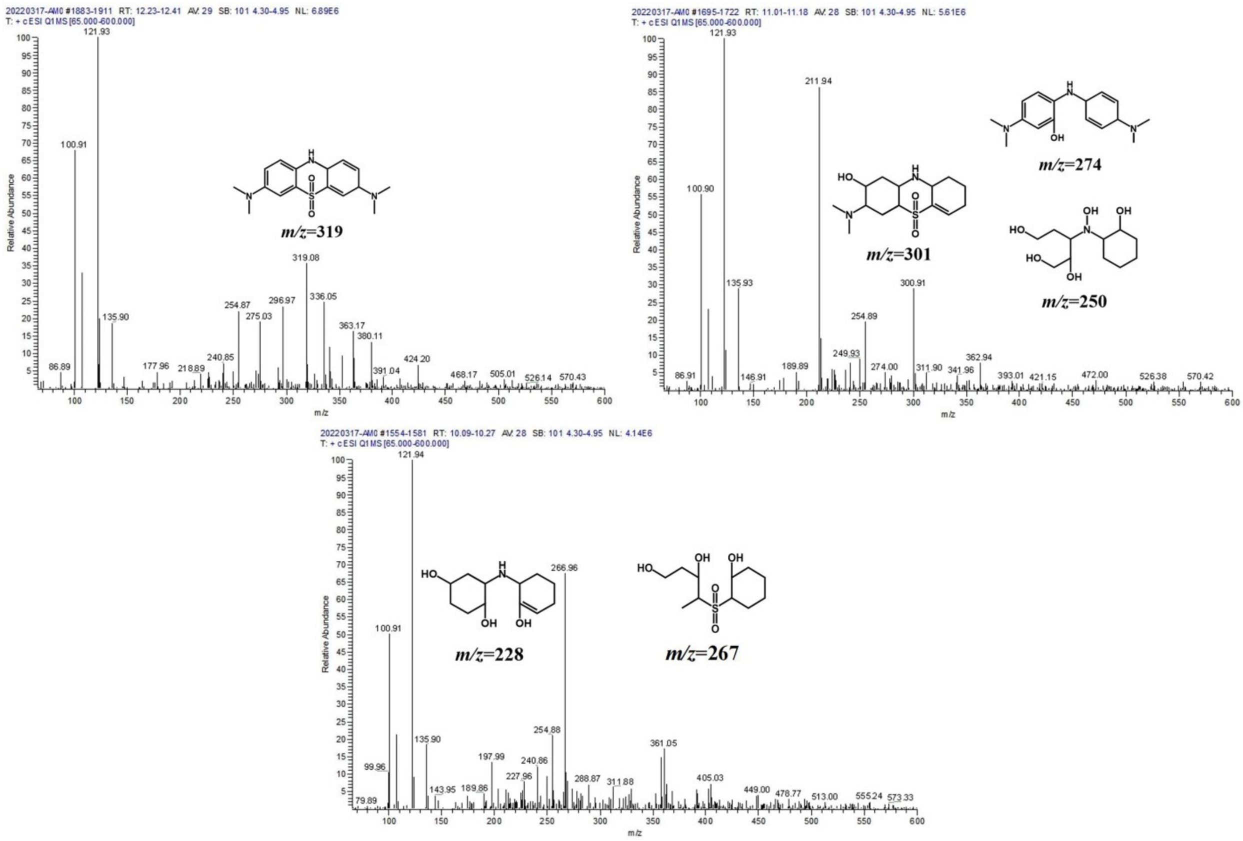

Fig. S2. Mass spectral database for decomposition products of MB over 20%AMO/BOB.

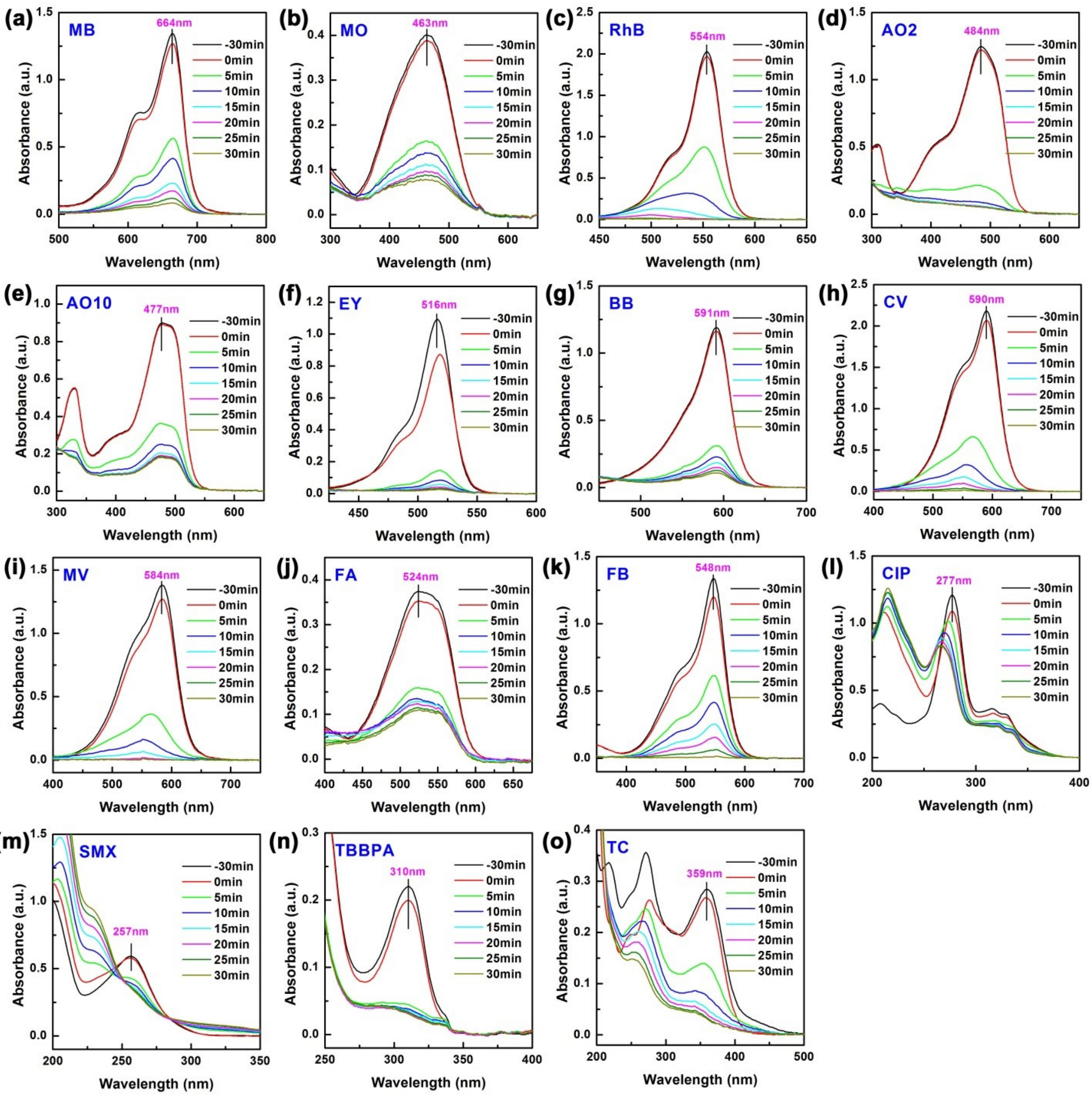

Fig. S3. UV-vis absorption spectra of various organic pollutants photodegraded by 20%AMO/BOB

($C_{\text{photocatalyst}}$ = 0.5 g L^{-1}, $C_{\text{pollutant}}$ = 10 mg L^{-1}).